AGU PUBLICATIONS

JGR

Journal of Geophysical Research: Solid Earth

RESEARCH ARTICLE
10.1002/2016JB013055

Key Points:
- First thermobarometry data in the Cordillera Blanca batholith indicates its emplacement in the upper crust (6–3 km) by sill underplating
- Tilting of the Cordillera Blanca batholith, footwall of the Cordillera Blanca normal fault
- Acceleration of exhumation rates over the past 2 Myr in the Cordillera Blanca synchronous with glaciations

Supporting Information:
- Supporting Information S1
- Table S1

Correspondence to:
A. Margirier,
audrey.margirier@univ-grenoble-alpes.fr

Citation:
Margirier, A., L. Audin, X. Robert, F. Herman, J. Ganne, and S. Schwartz (2016), Time and mode of exhumation of the Cordillera Blanca batholith (Peruvian Andes), *J. Geophys. Res. Solid Earth*, *121*, 6235–6249, doi:10.1002/2016JB013055.

Received 5 APR 2016
Accepted 5 AUG 2016
Accepted article online 10 AUG 2016
Published online 29 AUG 2016

©2016. American Geophysical Union. All Rights Reserved.

Time and mode of exhumation of the Cordillera Blanca batholith (Peruvian Andes)

Audrey Margirier[1], Laurence Audin[1], Xavier Robert[1], Frédéric Herman[2], Jérôme Ganne[3], and Stéphane Schwartz[1]

[1]Université Grenoble, Alpes, CNRS, IRD, ISTerre, Grenoble, France, [2]Institute of Earth Surface Dynamics, University of Lausanne, Lausanne, Switzerland, [3]Géosciences Environnement Toulouse, UMR CNRS-IRD-Université de Toulouse, Toulouse, France

Abstract The Cordillera Blanca batholith (12–5 Myr) forms the highest Peruvian summits and builds the footwall of the Cordillera Blanca normal fault (CBNF). Even if several models have been proposed, the processes driving both the exhumation of the Cordillera Blanca and extensional deformation along the CBNF are still debated. Here we quantify the emplacement depth and exhumation of the batholith of the northern Peru arc from the late Miocene to present. Based on a compilation of crystallization ages and new thermobarometry data in the Cordillera Blanca batholith, we propose that the batholith was emplaced at a depth of ~3 km in successive sills from 14 to 5 Ma. By contrast, the younger rocks exposed at the surface were emplaced the deepest (i.e., ~6 km) and are located close to the CBNF, suggesting post 5 Ma tilting. Furthermore, a formal inversion of the thermochronologic data indicates an increase of the exhumation rates in the Cordillera Blanca during the Quaternary. The higher predicted exhumation rates correlate with areas of high relief, both in the northern and central part of the Cordillera Blanca, suggesting that Quaternary valley carving by glaciations have a significant impact on the latest stage of the Cordillera Blanca exhumation (2–0 Ma).

1. Introduction

Subduction of the oceanic Nazca Plate beneath the continental South American plate is building the Andean range for more than 100 Myr. The uplift history and the present-day high elevations of the central Andes are the result of an important crustal thickening (60–80 km) [*James*, 1971; *Kono et al.*, 1989; *James and Snoke*, 1994; *Zandt et al.*, 1994]. For the past 30 years, several processes have been proposed to explain this crustal thickening, including: tectonic shortening [e.g., *Isacks*, 1988; *Kley and Monaldi*, 1998; *McQuarrie*, 2002], magmatic addition [e.g., *James and Sacks*, 1999], changes of the upper plate properties [e.g., *Isacks*, 1988], changes in the subduction interface [e.g., *Lamb and Davis,* 2003], changes in the subduction geometry [e.g., *Jordan et al.*, 1983; *Isacks*, 1988; *Gephart*, 1994; *Kley et al.*, 1999], delamination and crustal flow [*Husson and Sempéré*, 2003; *Garzione et al.*, 2006; *Schildgen et al.*, 2007], cratonic underthrusting [*Lamb and Hoke*, 1997], and erosion [e.g., *Masek et al.*, 1994; *Pope and Willett*, 1998; *Horton*, 1999; *Lamb and Davis,* 2003; *Barnes and Pelletier*, 2006]. The magmatic contribution to the crustal thickening is still discussed, but the present-day active arc in southern Peru represents at least a non-negligible contribution to the western Andes Miocene geomorphologic evolution [e.g., *James and Sacks*, 1999; *Mamani et al.*, 2010; *Boekhout et al.*, 2012]. No thermobarometric study has been performed in the Cordillera Blanca, whereas the late Miocene arc builds the highest Peruvian summits in this area (Cordillera Occidental, northern Peru) [*Mukasa*, 1984; *McNulty and Farber*, 2002; *Giovanni*, 2007].

The aim of this paper is to identify the causes of uplift and exhumation of the northern Peru late Miocene arc. In this area, the Cordillera Blanca batholith (14–5 Ma) [*Mukasa*, 1984; *McNulty and Farber*, 2002; *Giovanni*, 2007] builds the footwall of the 200 km long Cordillera Blanca normal fault (CBNF, Figure 1a) [*Bonnot et al.*, 1988] and its exhumation appears to be closely linked to the CBNF activity [*Bonnot et al.*, 1988; *Schwartz*, 1988]. However, the processes driving the exhumation of the Cordillera Blanca and extension along the CBNF are still debated. The extent to which both magmatism and normal faulting influenced Andean relief development is particularly unclear [e.g., *Margirier et al.*, 2015]. *Dalmayrac and Molnar* [1981], *Deverchère et al.* [1989], and *Petford and Atherton* [1992] suggested that extension resulted from gravitational collapse of a thickened crust, while *McNulty and Farber* [2002] suggested extension due to the arrival of the Nazca ridge beneath the Cordillera Blanca, increasing temporarily the coupling with the overriding plate. These

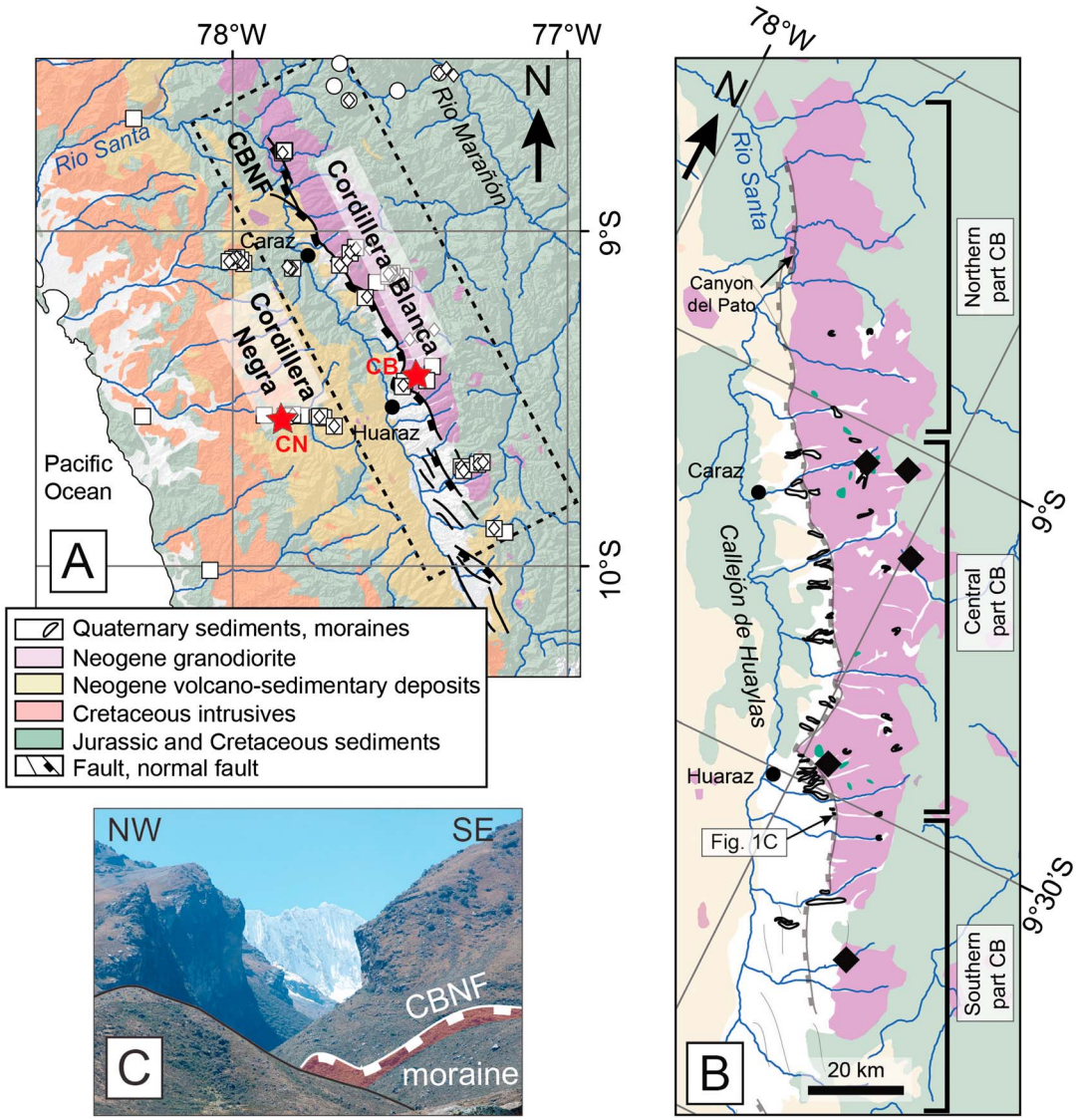

Figure 1. Geology of the Cordillera Blanca region. (a) Geological map of the Cordillera Occidental (northern Peru; modified from INGEMMET geologic map of Ancash) [*INGEMMET, El Instituto Geológico Minero y Metalúrgico*, 1999] showing location of low-temperature thermochronological data (white circles: zircon (U-Th)/He data; squares: apatite fission track; diamonds: (U-Th)/He data) [*Montario*, 2001; *Montario*, 2006; *Wipf*, 2006; *Giovanni*, 2007; *Hodson*, 2012; *Margirier et al.*, 2015; *Michalak et al.*, 2016]. Red stars point out the locations (CB and CN) of the tests of parameters for the inversion of thermochronologic data. (b) Simplified geological map of the Cordillera Blanca showing the batholith (pink), the contact between the batholith and Jurassic sediments (green), the CBNF (grey), the Canyon del Pato, the main moraines (black), and the thermobarometry sampling sites (black diamonds). (c) Photograph of the outlet of a U-shaped glacial valley (Quebrada Shallap).

models focused on the CBNF and did not explore the emplacement history of the Cordillera Blanca, its recent geomorphological evolution (5–0 Ma), or its present shape. Emplacement depths of the Cordillera Blanca batholith are not well constrained and have never been studied as a whole [*Wise and Noble,* 2003]. Its magmatic structure is also uncertain [*Egeler and De Booy*, 1956; *Cobbing et al.*, 1981; *Atherton and Sanderson*, 1987; *Petford and Atherton*, 1996]. On the basis of metamorphic mineral assemblages in the surrounding basement, the emplacement depth of the batholith is roughly estimated at ~9 km [*Petford and Atherton*, 1992; *McNulty et al.*, 1998]. In this paper, we report new amphibole thermobarometry data to quantify the emplacement depths across the batholith. We then estimate the total exhumation of the Cordillera Blanca batholith and the total displacement on the CBNF. Additionally, we constrain the recent evolution of the batholith by

modeling exhumation rates through time to discuss the geometry and role of the CBNF versus climate in the Cordillera Blanca exhumation.

2. Geological Context

The Cordillera Blanca consists of a young granitic pluton (14–5 Ma) [*Mukasa*, 1984; *McNulty and Farber*, 2002; *Giovanni*, 2007] emplaced in deformed Jurassic sediments of the Chicama Formation [*Atherton and Sanderson*, 1987]. The Cordillera Blanca batholith and its associated magmas, the Fortaleza and Yungay ignimbrites [*Farrar and Noble*, 1976; *Cobbing et al*., 1981; *Mukasa*, 1984; *Giovanni*, 2007], correspond to the last magmatic activity in northern Peru [*Petford and Atherton*, 1992]. The Cordillera Blanca batholith and associated volcanic rocks composition (high-Na, low heavy rare earth element, and high-Al with garnet residues) differs from typical calc-alkaline magmas [*Atherton and Sanderson,* 1987; *Petford and Atherton*, 1996; *Coldwell et al*., 2011]. These magmatic rocks display an adakitic signature indicating a high-temperature basaltic melt, i.e., either a source issued from thick underplated crust or from the subducting oceanic slab [*Petford and Atherton*, 1996; *Coldwell et al*., 2011]. The present-day data do not enable to decipher between these two sources. The Cordillera Blanca batholith is ~150 km long and trend parallel to the Andean range (Figure 1a). In the northern and central part, the total width of the batholith is more than 15 km (Figure 1b). In the southern part, the batholith is exposed sporadically within the Chicama sedimentary Formation [*Atherton and Sanderson*, 1987]. These sediments, metamorphosed at the contact with the batholith, are still preserved on some summits of the central and northern Cordillera Blanca (Figure 1b) [*Atherton and Sanderson*, 1987; *Wise and Noble*, 2003], indicating that the roof of the batholith is culminating today at ~6000 m (Figure 1) [*Wise and Noble*, 2003]. Since emplacement, the Cordillera Blanca batholith has been uplifted to reach 6000 m to build the highest Peruvian summit. Recent low-temperature thermochronologic data in the central part of the batholith suggest rapid (250°C/Ma) magmatic cooling of the batholith until 4 Ma and its subsequent exhumation (~1 mm/yr) between 4 and 0 Ma [*Margirier et al*., 2015]. This last exhumation stage is closely linked to the CBNF. The CBNF is a crustal-scale extensional structure characterized by ~1000 m high triangular facets and is responsible for a vertical relief over 4000 m: this fault shows at least 4500 m of vertical displacement since ~5.4 Ma [*Bonnot*, 1984; *Giovanni*, 2007]. Based on terrestrial cosmogenic nuclide dating of the main scarp, *Siame et al.* [2006] estimate a vertical slip rate of 3 ± 1 mm/yr, on the central part of the CBNF, for the last 3 kyr. *Giovanni* [2007], *Hodson* [2012], and *Margirier et al.* [2015] estimated exhumation rate of ~2 mm/yr, >1 mm/yr, and ~1 mm/yr, respectively, on the central part of the CBNF for the last 3 Myr based on low-temperature thermochronologic data. Triangular facets located in the northern and central parts of the Cordillera Blanca and the height of recent scarps decreasing southward suggest lower exhumation rates in the southern part of the Cordillera Blanca.

West of the Cordillera Blanca, the Callejón de Huaylas (Figure 1b), an elongated range-parallel intramountain basin (150 km long), separates the Cordillera Blanca and the Cordillera Negra. The first stratified series filling in this intramountain basin recorded its first episodes of tectonic subsidence associated to the CBNF initiation with some ignimbrites dated at 5.4 ± 0.1 Ma [*Giovanni*, 2007; *Giovanni et al*., 2010]. The Cordillera Negra (~4500 m) builds the hanging wall of the CBNF. This range consists of Cretaceous and Paleogene plutons (73–48 Ma) [*Mukasa and Tilton*, 1984; *Beckinsale et al*., 1985] intruded in the Chicama Formation. Neogene volcano-sedimentary deposits capped the older formations in its southern part.

3. Glacial Valleys Morphology in the Cordillera Blanca

Past Quaternary glaciations had a strong imprint on the Cordillera Blanca landscape [*Clapperton*, 1983; *Rodbell*, 1993]. *Farber et al.* [2005], *Rodbell* [1993], and *Smith et al.* [2005] suggested extensive pre–Late Glacial Maximum (pre-LGM) glaciation in the Cordillera Blanca, the Cordillera Oriental and Junin basins (respectively since at least 400 kyr, 500 kyr, and 1.4 Myr). Conspicuous geomorphic glacial features such as U-shaped valleys are observed on the western flank of the Cordillera Blanca batholith (Figure 1c). Several relicts of moraines and some striated roches moutonnées can also be found on the flanks and outlet of these valleys (Figures 1b and 1c). The Cordillera Blanca relief is directly linked to the depth of the valleys carving of the batholith. The relief, calculated as the difference between the maximum and the minimum altitude, is approximated with swath profiles of ~10 km and ~30 km width (Figure 2). In Figure 2, the distance between the blue and the green lines represents an approximation of the local relief. The maximum relief is located in

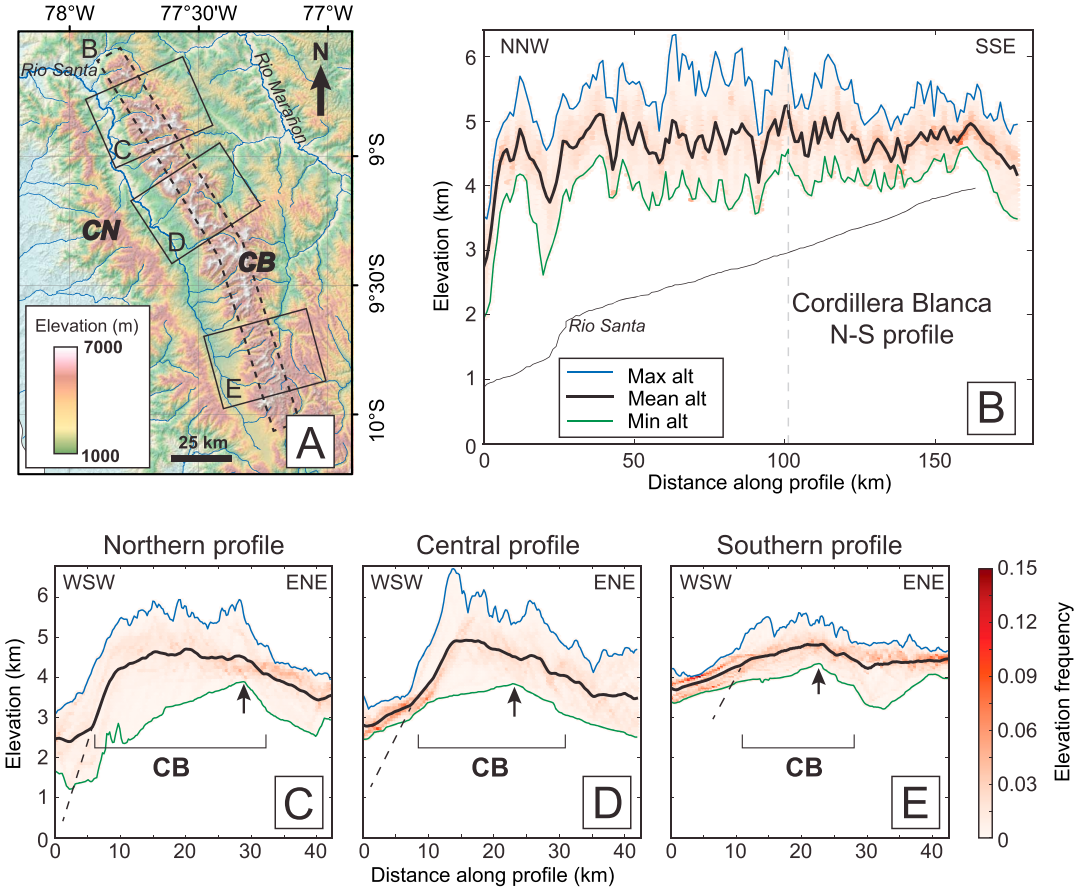

Figure 2. Elevation and relief of the Cordillera Blanca. (a) Topographic map showing the Cordillera Blanca (CB), the Cordillera Negra (CN), and the location of the swath profiles that are extracted from the 90 m SRTM digital elevation model V4.1 (width of the swath is 10 km for N-S profile and 30 km for E-W profiles). (b) Cordillera Blanca N-S profile (profile width ~10 km) and (c–e) E-W profiles in the northern, central, and southern parts of the Cordillera Blanc showing the maximum (blue line), mean (black line), and minimum (green line) elevation (profiles width ~30 km).

the central and northern parts of the Cordillera Blanca (~3 km; Figure 2). Most of the 6000 m high summits are located in the northern and central part of the Cordillera Blanca, reaching a maximum in central part (Figure 2b). Even if the mean elevation of the southern part of the Cordillera Blanca is higher than in the northern part, relief is lower (~1 km; Figure 2). In the central and northern parts of the Cordillera Blanca the large relief (~3 km) suggests substantial valley carving due to glacial erosion. In the southern part, lower relief suggests less glacial erosion. Relief and maximum elevation are also larger on the western flank (~3 km, 6500 m) than in the eastern flank (~2 km, 6000 m) in the central part of the Cordillera Blanca indicating more incision in the western flank (Figures 2c–2e).

4. Methods

4.1. Amphibole Thermobarometry

Amphibole thermobarometry has been widely used to estimate both the emplacement pressure and temperature of calc-alkaline igneous rocks [e.g., *Costa et al.*, 2013; *Turner et al.*, 2013; *Brenna et al.*, 2014; *Leuthold et al.*, 2014; *Ridolfi et al.*, 2016]. In this study, we applied the thermobarometric method introduced by *Ridolfi and Renzulli* [2012], which is calibrated for calc-alkaline and alkaline igneous rocks for pressure ranging from 1.3 to 22 kbar (hereafter RR2012). RR2012 takes in account the composition of Mg-rich calcic amphiboles (total atoms per formula units of Si, Ti, Al, Fe, Mn, Mg, Ca, Na, and K, on the basis of 13 cations) [e.g., *Ridolfi et al.*, 2010] to calculate pressure and temperature conditions of magmatic crystallization. A chemical trend is classically observed for the clino-amphibole with the most Si-depleted composition

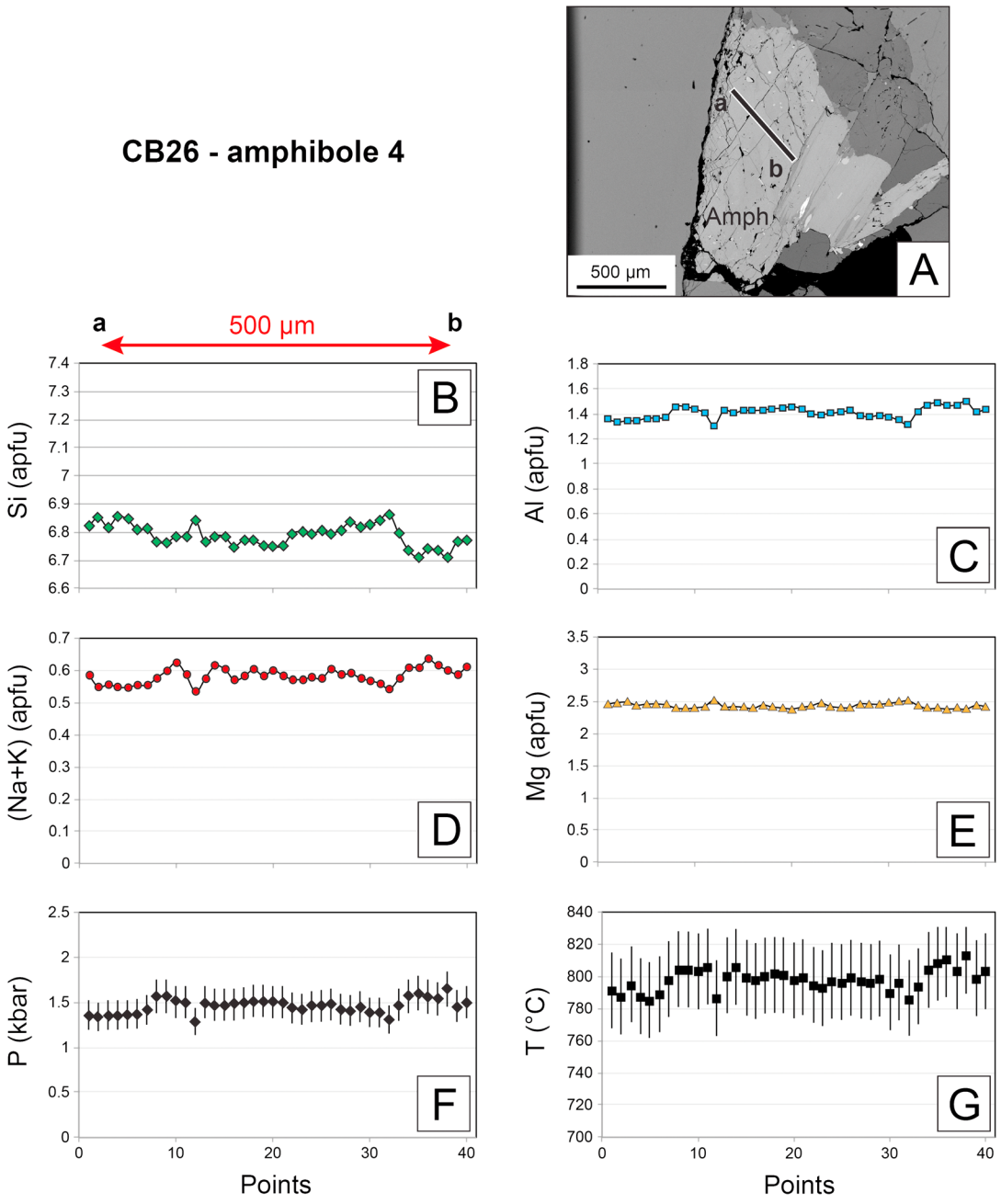

Figure 3. (a) Representative microprobe image of an amphibole crystal of sample CB-26 showing the performed analytical transect a-b. (b–e) Chemical composition of the amphibole along the transect a-b. (f, g) Pressure and temperature obtained along this transect using RR2012 thermobarometric method [*Ridolfi and Renzulli*, 2012] (symbol bars indicate the standard error of the method (i.e., 12% for pressure and 24°C for temperature)).

(ferro-pargasite or ferro-tschermakite end-members according to the $(Na + K)_A$ value) [*Leake et al.*, 1997; *Ridolfi et al.*, 2010], which are characterized by high-Fe contents, whereas Si-enriched amphiboles (magnesio-hornblende or edenite) are characterized by elevated Mg contents (Figure 3). We sample the granite of the Cordillera Blanca batholith across strike, and apart from the faulted gouge and the mylonitized rocks (see Figure 1b for sampling location) to obtain the emplacement depth and temperature of the batholith without any influence of ductile or brittle tectonic deformation. Chemical data collected on magmatic amphiboles were filtered on the base of pressure-related "apparent percentage error" (APE) values calculated with the

RR2012 thermobarometric method. Following recommendations by the authors, we fixed a maximum of 50 for the APE to retain or exclude the data for pressure and temperature calculations (first filter: moderate confidence level). We also applied a second filter (high-confidence level) to exclude amphiboles whose chemistry did not match the dedicated range of chemical composition and structural formulae. It is also worth pointing that the amphibole barometer of *Ridolfi and Renzulli* [2012] has been under scrutiny recently [e.g., *Walker et al*., 2012; *Shane and Smith*, 2013; *Erdmann et al*., 2014; *Kiss et al*., 2014]. Some authors have proposed that the estimated pressures are very sensitive to variations in melt composition [*De Angelis et al*., 2013; *Shane and Smith*, 2013; *Erdmann et al*., 2014]. However, amphibole barometry of *Ridolfi and Renzulli* [2012] gives satisfactory results when compared to experimental results from a broad range of starting compositions (basalt to rhyolite) and pressures (200–800 MPa) [*Putirka*, 2014] and to other thermobarometric constraints [*Ridolfi et al*., 2016]. In situ major element abundances were measured on thin section with an electron microprobe JEOL JXA-8230 at ISTerre (Grenoble), operating condition were 15 kV and 12 nA. The amphiboles were analyzed in spot mode (1 μm diameter). See supporting information files for additional information on the application of amphibole thermobarometry.

4.2. Crystallization Ages and High-Temperature Thermochronology Ages

We compile data from the Cordillera Blanca batholith for geochronometers and high-temperature (>300°C) thermochronometers: zircon U-Pb, hornblende K-Ar, hornblende Ar-Ar, muscovite and biotite Rb-Sr, and muscovite and biotite K-Ar/Ar-Ar which have closures temperature ranging from 800°C to 300°C [*Giletti and Day*, 1968; *Stewart et al*., 1974; *Wilson*, 1975; *Cobbing et al*., 1981; *Mukasa*, 1984; *Beckinsale et al*., 1985; *Giovanni*, 2007]. These geochronometers provide crystallization and cooling ages. They enable us to quantify both the chronology and the dynamics of the batholith emplacement in the crust.

4.3. Inversion of the Thermochronologic Data

We formally invert the extensive set of thermochronometric and geobarometric data (zircon fission track and (U-Th)/He, apatite fission track and (U-Th)/He) [*Montario*, 2001; *Montario*, 2006; *Wipf*, 2006; *Giovanni*, 2007; *Hodson*, 2012; *Margirier et al*., 2015; *Michalak et al*., 2016; this study] to quantitatively estimate the exhumation history, using data shown in Figure 1a. We used the method proposed by *Fox et al.* [2014] and modified by *Herman and Brandon* [2015]. This procedure involves a weakly nonlinear least squares inversion and allows efficient treatment of a large number of spatially distributed data. This method exploits the information contained in both age-elevation profiles and multithermochronometric systems strategies. In this approach, several parameters must be tested to ensure that the inferred exhumation rates are robust. We refer the reader to *Fox et al.* [2014] for an in-depth discussion on each of these parameters. First, the depth to the closure temperature is expressed as the integral of exhumation rate from the thermochronometric age to present day. The integral is discretized in a series of fixed time steps (Δt), which must be selected. Second, the depth of the closure isotherms is calculated using a one-dimensional thermal model that includes a correction for the effects of topography. We tested the impact of the thermal model by changing the bottom boundary conditions (T). Third, the method assumes that the samples are spatially correlated through a correlation function that includes a variance (σ). Finally, the calculated exhumation rates represent a deviation from an a priori exhumation ($\dot{e}_{pr}$) rate that is updated to posterior exhumation rates. We show in Figure 4 the impact of changing Δt, T, and $\dot{e}_{pr}$ assess on the estimated exhumation history. The solution is shown at two selected locations on either side of the fault.

5. Results

5.1. Thermobarometry in the Cordillera Blanca Batholith

As evidenced on thin sections and microprobe images, the samples show only low deformation at crystalline scale (Figure 3a). Amphibole crystals are not abundant in the Cordillera Blanca batholith; only 5 of our 20 samples contain amphiboles. We performed microprobe analysis along rim to rim transect on at least three amphiboles by sample (Figure 5a and Table S1 in the supporting information). After the application of the two filters of the RR2012 method, we discarded ~15% of the calcic amphiboles. Estimated emplacement pressure ranges from 0.9 ± 0.1 to 2.6 ± 0.3 kbar, at a temperature of 720–800°C (Table 1 and Figure 5a). The elevation range of the samples is very small (from 3928 m to 4247 m); there is no relationship between present-day elevation and emplacement pressure (Figure 5b and Table 1). Calculated depths (using an average rock

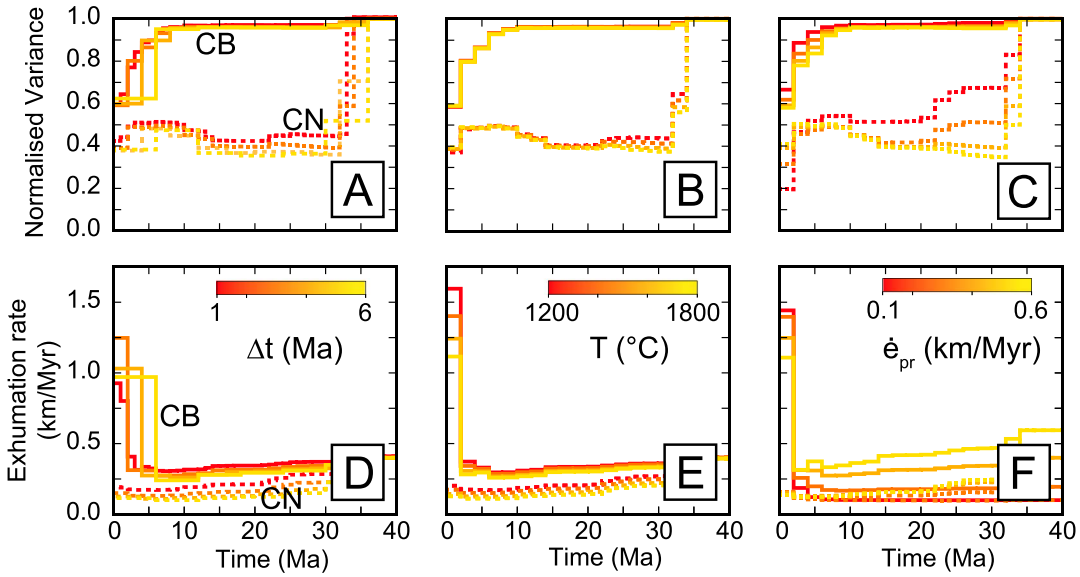

Figure 4. Sensitivity of exhumation rate to different parameters. The location of the two points (CB and CN) is shown Figure 1 by red stars. (a–c) Normalized variance for each exhumation history; the lower the normalized variance is, the better the inversion is constrained. (d–f) Exhumation rate history for a range of Δt, T, and $\dot{e}_{pr}$ [*Fox et al.*, 2014; *Herman and Brandon*, 2015].

density of 2.7 g/cm^3) indicate that the Cordillera Blanca batholith emplaced at shallow crustal level, i.e., between 3.1 and 6.3 km. Pressure estimations vary spatially along and across the batholith. Close to the CBNF the emplacement pressures are high (southwest of the Cordillera Blanca batholith; 2.3 ± 0.3 kbar); they decrease with distance from the fault (northeast of the batholith; 1.2 ± 0.1 kbar) (Figure 6b).

5.2. Crystallization and Cooling Ages

Crystallization and cooling ages ($T_c > 300$°C) range from 30 ± 0.0 to 3.3 ± 1.2 Ma in the Cordillera Blanca batholith (Figure 6a). Some muscovite Rb-Sr and zircon U-Pb ages are significantly older than other published ages in the same area, which makes it difficult to quantify the crystallization and cooling of the Cordillera

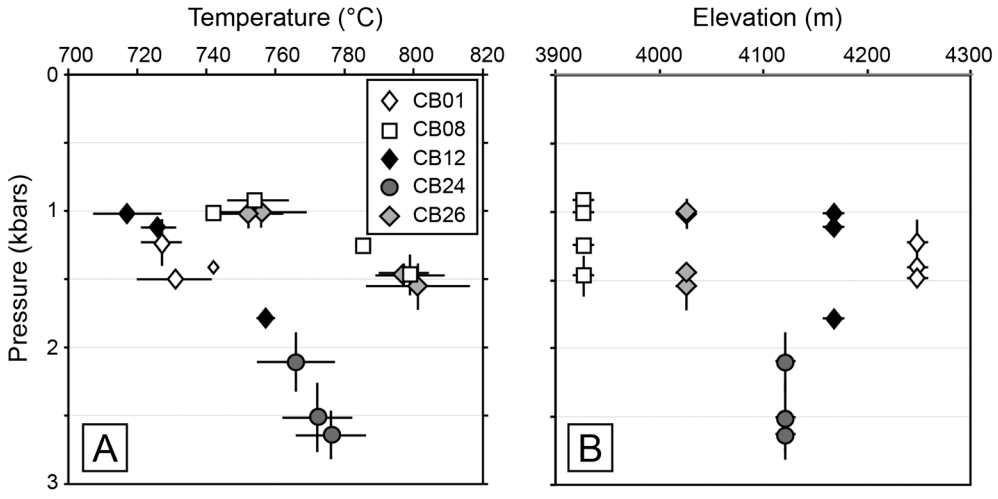

Figure 5. (a) Magmatic pressure versus temperature calculated for the Cordillera Blanca batholith using the thermobarometer of *Ridolfi and Renzulli* [2012]. Each point represents estimates based on averages of multiple analyses within an individual amphibole crystal (Table 1; 12 analyses per amphibole in average). Bars indicate errors (1σ) due to multiple analyses of each amphibole; smaller symbol reports the result of single analysis. (b) Magmatic pressure versus present-day elevation and magmatic pressure for each amphibole crystal.

Table 1. Average Amphibole Compositions and Thermobarometric Data Calculated Using the Method of RR2012[a]

Sample	Amphibole	*N*	SiO_2	TiO_2	$Al2O_3$	$Cr2O_3$	FeO	MnO	MgO	CaO	Na_2O	K_2O	APE	*T* (°C)	*P* (MPa)
CB01	1	3	47.50	0.79	7.40	0.00	19.34	0.41	10.66	10.13	0.89	0.28	46	727	123
CB01	2	2	46.68	0.81	8.71	0.01	19.17	0.40	10.06	10.87	1.01	0.36	51	730	150
CB01	3	1	47.46	0.90	8.06	0.00	18.76	0.42	10.84	10.30	0.96	0.23	47	742	142
CB01	4	0	-	-	-	-	-	-	-	-	-	-	-	-	-
CB08	1	3	47.23	1.08	7.34	0.00	15.34	0.62	12.62	11.63	1.42	0.69	9	785	125
CB08	2	3	48.23	0.78	6.47	0.01	15.66	0.64	12.59	11.85	0.99	0.61	25	742	101
CB08	3	5	48.48	0.68	5.95	0.01	15.16	0.67	13.26	11.77	1.19	0.56	6	755	92
CB08	4	18	46.05	1.21	8.22	0.01	15.94	0.56	12.04	11.65	1.54	0.86	18	798	147
CB12	1	0	-	-	-	-	-	-	-	-	-	-	-	-	-
CB12	2	2	45.42	1.27	9.31	0.05	19.33	0.45	9.41	10.89	1.03	0.46	48	757	179
CB12	3	3	48.80	0.66	6.73	0.01	18.97	0.58	11.32	10.37	0.63	0.28	49	726	112
CB12	4	0	-	-	-	-	-	-	-	-	-	-	-	-	-
CB12	5	4	48.80	0.72	6.48	0.01	18.74	0.52	11.36	10.55	0.75	0.27	49	717	102
CB24	1	24	42.34	0.67	11.24	0.01	21.94	0.64	7.11	11.59	1.38	1.37	20	772	251
CB24	2	17	41.88	0.65	11.51	0.01	22.30	0.63	6.79	11.52	1.48	1.44	30	776	264
CB24	3	12	43.16	0.77	10.42	0.03	21.71	0.66	7.45	11.59	1.41	1.21	20	766	210
CB26	1	20	48.39	0.86	6.33	0.01	16.21	0.76	12.32	11.65	1.16	0.61	7	756	101
CB26	2	16	48.31	0.80	6.42	0.02	16.25	0.75	12.29	11.74	1.10	0.59	9	752	102
CB26	3	15	45.83	1.42	8.37	0.01	17.10	0.69	11.01	11.57	1.47	0.93	20	801	155
CB26	4	28	46.01	1.33	8.13	0.01	17.24	0.71	11.06	11.53	1.47	0.86	22	797	146

[a]*N*: number of spot analyses; APE: apparent pressure error (see RR2012); *T*: calculated temperature; *P*: calculated pressure. RR2012 errors are ±24°C for T and ±12% for P.

Blanca batholith. *Giovanni* [2007] proposed that ages >25 Ma may correspond to zircon recycling. The GPS coordinates of the muscovite Rb-Sr samples are not accurate; as they are close to the CBNF they may be located in the hanging wall of the fault. Thus, we exclude these ages for our interpretation.

Along strike, ages are younger in the central and northern parts of the Cordillera Blanca batholith (4–7 Ma), and older (~14 Ma) in the southern tip of the granite. Across-strike crystallization ages increase away from the CBNF, in the central part of the batholith (Figures 6a and 6c). The young emplacement ages distributed in the vicinity of the fault correspond to high-pressure crystallization conditions of the batholith (Figure 6), and both criteria are found where the granitic outcrop is the thickest (i.e., western flank of the central and northern parts of the batholith).

5.3. Inversion of Thermochronologic Data

Modeling of thermochronologic ages [*Fox et al*., 2014] from northern Peru reveals space-time variations in exhumation rates over the past 20 Ma (Figure 7). A normalized variance close to 1 indicates a high uncertainty. We can only constrain the rates at the timescale provided by the measured ages. For the Cordillera Negra the low variance (<0.5) indicates that our data provide constrain on erosion rates for at least 30 Myr (Figure 7b). From 40 to 10 Ma, the value of the Cordillera Blanca normalized variance close to 1 indicates poorly constrained exhumation rates (Figures 7b and 7c). Since 10 Ma, the data from the Cordillera Blanca provide constraint on exhumation rates, the variance decrease so we can interpret exhumation rate values (Figure 7b). Modeled exhumation rates are almost constant in the Cordillera Negra for the last 30 Myr with an average rate at ~0.2 km/Myr (Figure 7c). In the Cordillera Blanca, the exhumation rates increased from ~0.3 km/Myr at 10 Ma to ~1.0 km/Myr at the present day (Figure 7c).

Modeled exhumation rates are much higher in the Cordillera Blanca (5 times) than in the Cordillera Negra for the last 6 Ma (Figure 7c). Exhumation rates are higher in the central part of the Cordillera Blanca than in the southern and the northern tips of the batholith, where the granite is still caped by the sedimentary country rocks (Figure 1). Our most striking result is that exhumation rates increase over the past 5 Myr with a small acceleration at ~5 Ma in the southern part of the Cordillera Blanca followed by a strong acceleration of exhumation rates over the past 2 Myr (Figure 7c). In the Cordillera Blanca exhumation rates increase from ~0.25 mm/yr, between 6 and 4 Ma, to ~1 mm/yr, between 2 and 0 Ma, where young ages (i.e., < 2 Ma) are observed (Figure 7c). In the Cordillera Negra and in the Marañon region, results indicate a mean exhumation rate of 0.2 mm/yr for the last 30 Ma (Figure 7).

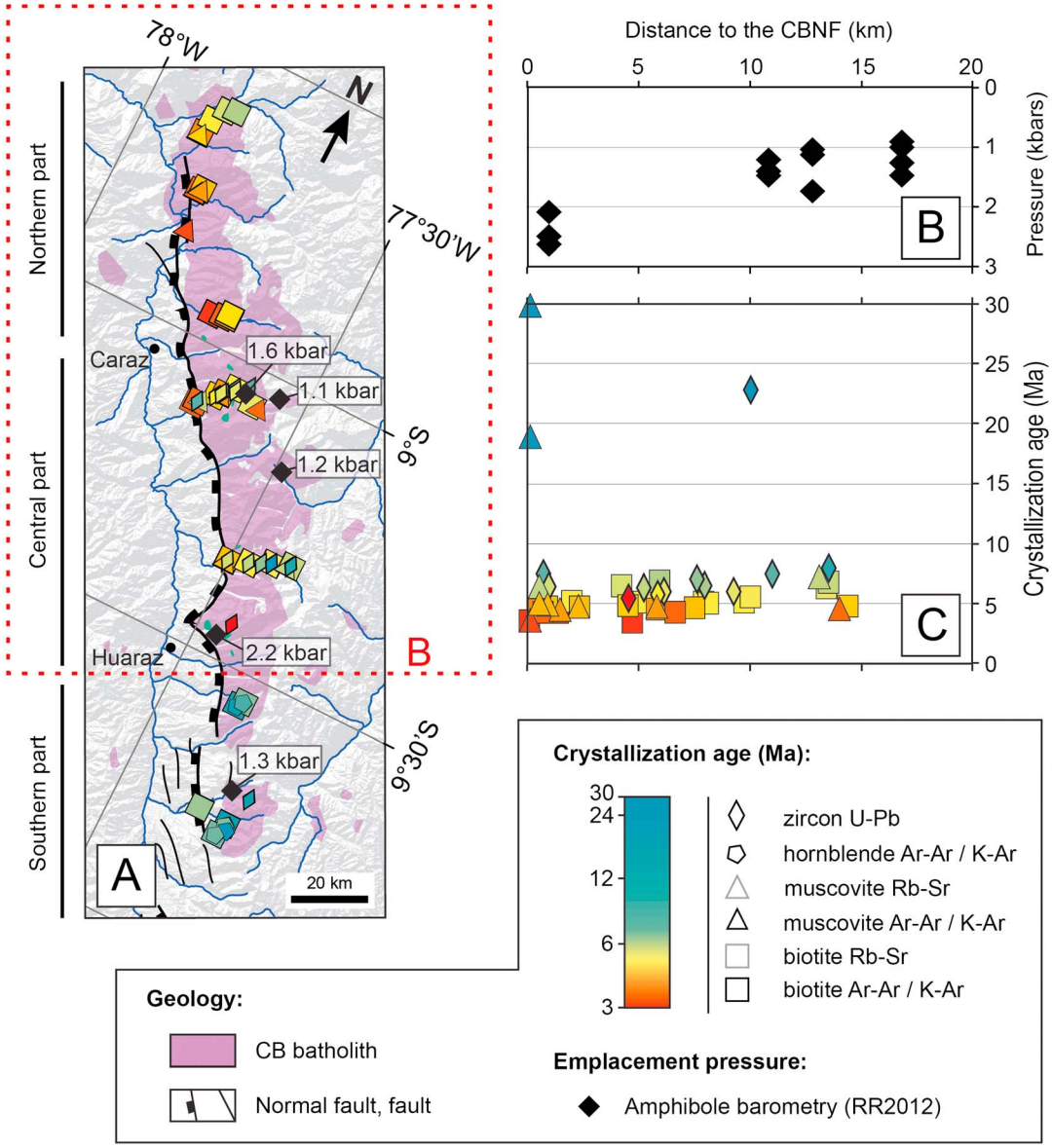

Figure 6. Spatial distribution of magmatic pressures and cooling ages. (a) Map showing the cooling ages (colored symbols) and the emplacement pressure (black diamonds) of the Cordillera Blanca batholith. (b) Magmatic pressure (black diamonds) versus distance from the CBNF. Magmatic pressures were calculated for the Cordillera Blanca batholith using the thermobarometer of *Ridolfi and Renzulli* [2012]. (c) Crystallization and cooling ages versus distance to the CBNF [*Stewart et al.*, 1974; *Wilson*, 1975; *Cobbing et al.*, 1981; *Mukasa*, 1984; *Beckinsale et al.*, 1985; *McNulty et al.*, 1998; *Giovanni*, 2007].

6. Discussion

6.1. Emplacement Depth and Magmatic Structure of the Cordillera Blanca Batholith

Thermobarometry data suggest emplacement of the Cordillera Blanca batholith between 3.1 ± 0.3 and 6.3 ± 0.8 km depth. These depths indicate that the roof of the Cordillera Blanca batholith was emplaced at ~3 km (close to the sediments in the eastern and southern part of the Cordillera Blanca). In contrast, in the central part of the Cordillera Blanca, in the vicinity of the fault, pressure is greater and reaches 6.2 ± 0.8 km (Figure 6). The observed depths are lower than pressure estimates by previous studies (>6 km) based on metamorphic mineral assemblages in the contact metamorphic aureole [*Petford and Atherton*, 1992; *McNulty and Farber*, 2002]. However, the calculated depths are compatible with metamorphic mineral assemblages described by *Petford and Atherton* [1992]. They indicate an emplacement at shallow crustal level

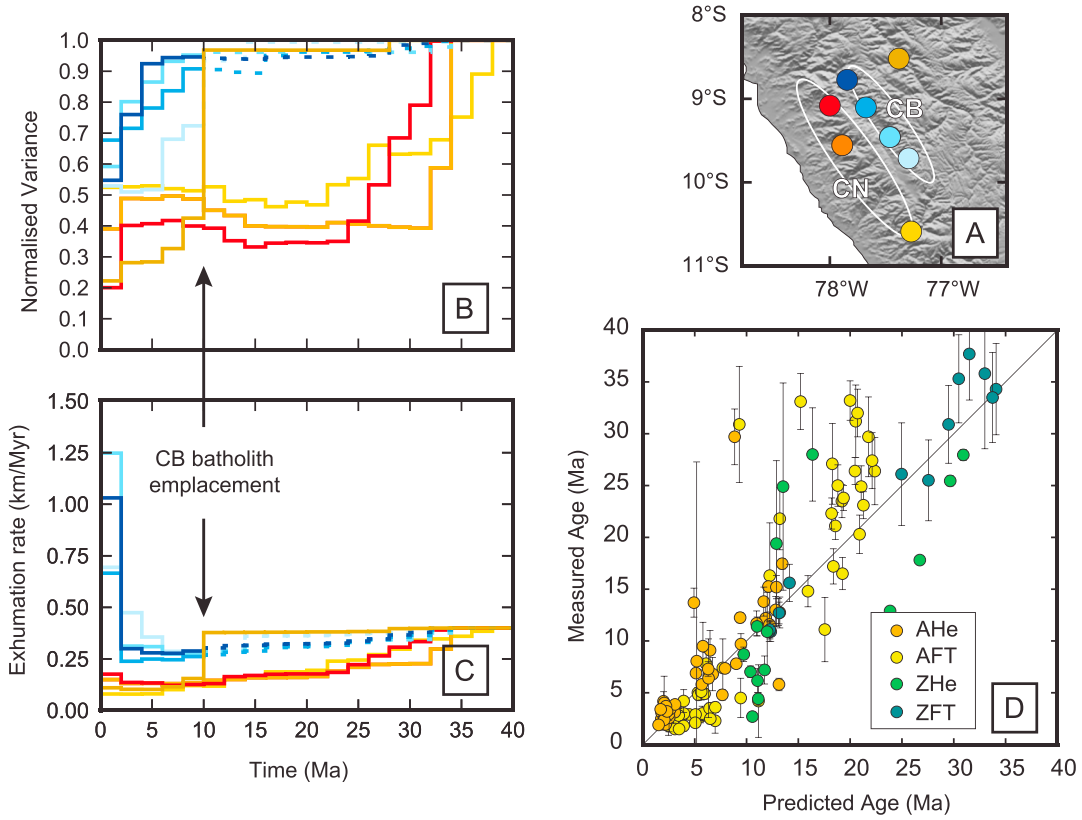

Figure 7. (a) DEM with location of the exhumation rate. Colors of the points are used in Figures 7b and 7c to track each sample. (b) Variance of the exhumation rate inversion for the different locations. (c) Exhumation rate versus time for the different points. Model parameters include an a priori exhumation rate of 0.4 ± 0.2 km/Myr, an exponential correlation function with length scale of 20 km, and an initial geothermal gradient of 32°C/km. The calculation was done for 2 Myr time steps. (d) Misfit of the inversion.

consistent with the low assimilation of country rocks and the sharp contact [*Petford and Atherton*, 1992]. Our amphibole barometry results (3.1–6.3 km depth) indicate that the granite was emplaced at greater depth, close to the CBNF, suggesting more exhumation in the vicinity of the fault and a tilt of ~15° of the Cordillera Blanca batholith since its emplacement (equation (1) and Figure 8).

$$\alpha = \tan^{-1}\left(\frac{6.3 - 3.1}{15}\right) \approx 15° \quad (1)$$

The emplacement depth of the Cordillera Blanca batholith obtained close to the CBNF (6.3 km) indicates that there is at least ~6 km of footwall uplift close to the CBNF assuming a regional mean elevation of ~4000 m during the batholith emplacement [*Hoorn et al.*, 2010]. The Lloclla Formation (fluvio-torrential and fluvio-glacial conglomerates) filled the Callejón de Huaylas located in the hanging wall of the CBNF since at least 5.4 Myr. In addition, *Giovanni et al.* [2010], based on the thickness of this formation, proposed at least 1300 m of basin subsidence since 5.4 Ma in the Callejón de Huaylas. Using a 40° dipping fault plane, these vertical offsets (6 km + 1.3 km) correspond to a displacement of ~11.4 km on the ~40° dip CBNF coherent with previous estimations from *Wise and Noble* [2003].

Our compilation of crystallization ages and high-temperature thermochronologic data indicates that cooling ages are younger close to the CBNF, where the exhumation of the granite is more important (central part of the Cordillera Blanca). *Petford and Atherton* [1992] already showed this trend and suggested three hypotheses: they are due (i) to magmatism migration toward the east or (ii) to heating/slow cooling close to the fault or (iii) to argon loss in the deformed zone. Instead, our data suggest that this trend reflects variations in the chronology and depth emplacement of the batholith, recorded by series of sills. First, the magma crystallized at

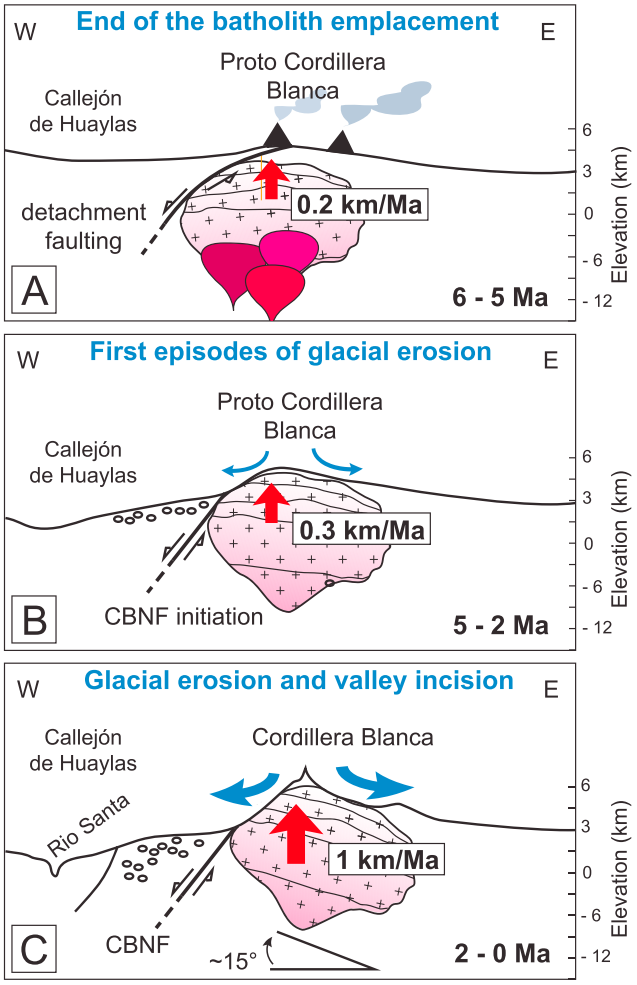

Figure 8. Schematic W-E cross section of the Cordillera Blanca and the CBNF. (a) 6–5 Ma: Final stage of the Cordillera Blanca emplacement; detachment faulting. (b) 5–2 Ma: CBNF initiation, Cordillera Blanca exhumation along the CBNF, deposit of the first residuals eroded from the CB in the Callejón de Huaylas. (c) Glacial valley incision, increase of exhumation rates, and tilting of the Cordillera Blanca batholith.

shallow crustal depth and then the following magmas emplaced as sills below the first one (Figure 8). Large intrusions usually emplaced as a succession of sills as the Torres del Paine, the Sierra Nevada batholith in the American Cordilleras or the Cho Oyu, and the Everest in Himalaya [e.g., *Sisson et al.*, 1996; *Searle*, 1999; *Leuthold et al.*, 2012]. Moreover, the high temperature of the batholith emplacement (750 ± 25°C) and the normal ductile shear sense observed in the western flank of the batholith and at the sediments/granite contact in the Canyon del Pato [*Petford and Atherton*, 1992] indicate that the Cordillera Blanca batholith emplacement is synchronous with ductile deformation on the western flank of the Cordillera Blanca batholith. We suggest that the ductile deformation controlled the initiation of the batholith slow exhumation as evidenced by low exhumation rates at that time (Figure 8a).

Afterward, when the magma production decreased and the magmatic body cooled, the CBNF initiated along its western flank. We suggest that the development of the CBNF in brittle conditions built 1 km high tectonic scarps and relief (Figure 8b). Finally, the Cordillera Blanca has been tilted toward the east, exhuming younger rocks that have crystallized deeper close to the CBNF (Figure 8c). Considering the low elastic thickness of the crust in the Cordillera Blanca area [*Pérez-Gussinyé et al.*, 2009] and the Cordillera Blanca magmatism which may favor ductile deformation in the lower crust since ~12 Ma, we suggest that a cantilever planar fault model with flexural response of the upper crust explain both the footwall uplift and tilting [*Kusznir et al.*, 1991]. In this model, the tilting of the Cordillera Blanca is directly controlled by the elastic thickness of the crust. However, we cannot exclude a rolling hinge model for the CBNF [e.g., *Buck*, 1988; *Giovanni*, 2007; *Campani et al.*, 2010].

6.2. Exhumation of the Cordillera Blanca Along the CBNF

The exhumation rates obtained for the Cordillera Blanca are in the same order of magnitude than those obtained by *Giovanni* [2007], *Hodson* [2012], and *Margirier et al.* [2015] for the last 3 Myr and *Schwartz* [1988] on a more recent timescale (3000 years). Our results also suggest an increase of exhumation rate during the last 2 Ma in agreement with *Giovanni* [2007]. The emplacement of the Cordillera Blanca at shallow crustal levels and the exhumation rate modeling through time indicate that the Cordillera Blanca exhumation is delayed compared to the batholith emplacement (emplacement at 9–4 Ma, exhumation at 5–0 Ma; Figures 6 and 7). Based on the late exhumation rate increase, and in agreement with *Giovanni et al.* [2010], we suggest that the Cordillera Blanca exhumation is not driven by the batholith emplacement as previously proposed by *Petford and Atherton* [1992].

Provenance analysis and WNW paleocurrent directions in the Lloclla Formation (Callejón de Huaylas) recorded the first erosion of the Cordillera Blanca granite marking its surface outcrop in the southern part of the Cordillera Blanca batholith at 6.4 Ma [*Bonnot*, 1984; *Giovanni*, 2007]. It suggests, in agreement with our data, that the exhumation initiated in the southern part of the Cordillera Blanca and then propagated northward (Figure 7). We propose that the exhumation increase from 5 Ma in the southern part of the Cordillera Blanca is related to the initiation of the CBNF at the end of the batholith emplacement (~5.4 Ma) and consequent relief building [*Bonnot*, 1984; *Giovanni et al*., 2010]. The presence of granitic polished clasts in the fluvio-glacial LLoclla formation signs Pliocene glacial erosion of the Cordillera Blanca [*Bonnot*, 1984]. Moreover, the central part of the Cordillera Blanca exhibits the most conspicuous glacial features (cf. depth of glacial valleys), corresponding to the higher exhumation rate from 2 Ma (Figure 7). The rapid increase of the exhumation rates over the past 2 Ma could correspond to the glacial valley carving since 1.4 Myr (Figure 7) [*Smith et al*., 2005]. In addition, there is a possibility that the late increase in exhumation rate was related to a change in the regional base level related to the Canyon del Pato incision [*Giovanni*, 2007] in the northern part of the Callejón de Huaylas. Considering that (1) the higher exhumation rates are located in the central part of the Cordillera Blanca that is not yet reach by headward erosion of the Rio Santa (Figures 2 and 7), (2) the Cordillera Blanca morphology is strongly glaciated with U-shaped valleys and numerous glacial features [*Clapperton*, 1983; *Rodbell*, 1993], and (3) extensive glaciations have been documented for at least 0.5 Myr [*Rodbell*, 1993; *Farber et al*., 2005; *Smith et al*., 2005], we favor the glacial erosion to explain the late increase of exhumation rates in the Cordillera Blanca in agreement with global analysis [*Zhang et al*., 2001; *Herman et al*., 2013]. Climate change could have induced larger and more durable glaciations in the Cordillera Blanca during the Quaternary [*Farber et al*., 2005]. *Farber et al.* [2005] dated moraines $>$400 ka, these moraines located at low elevations demonstrate that the most extensive glaciation in the Cordillera Blanca did not occur at the end of the last glacial. They also documented two separate late glacial advances at 29 ka and 16.5 ka. Several authors suggested that glaciers are more effective erosional agents than rivers and that glaciations favored valley enlargement and deepening [e.g., *Valla et al*., 2011; *Montgomery*, 2002], and glaciations had significant impact on mountain erosion during the Quaternary [e.g., *Zhang et al*., 2001; *Herman et al*., 2013]. In the Cordillera Blanca, our results suggest that the glacial valley carving could have contributed to increase the relief with valley lowering (glacial incision) and preservation of the high summits. In addition, the erosional unloading associated to glacial erosion likely induced isostatic rebound and additional rock uplift and exhumation [e.g., *Champagnac et al*., 2007]. Finally, the increase in surface elevation increases the active glaciers accumulation areas resulting to enhanced glacial erosion [e.g., *Braun et al*., 1999].

7. Conclusions

Emplacement age compilation indicates that the Cordillera Blanca batholith emplaced from 14 to 5 Ma. This first compilation shows a trend in crystallization ages, with the younger ages (~5 Ma) located in the central part of the Cordillera Blanca, close to the CBNF. Additionally, we present the first thermobarometry data from the Cordillera Blanca batholith. These new data show a shallow emplacement of the magma in the crust (~3 km) and indicates that the batholith crystalized at greater pressure, close to the CBNF (~6 km). Based on these data, we propose that the batholith emplaced in successive sills from 14 to 5 Ma and have been tilted after ~5 Ma. The shallow emplacement of the batholith (~3 km) questions the use of high-temperature thermochronometers to quantify exhumation rates in the Cordillera Blanca. The inversion of the thermochronometric and geobarometric data points out a significant increase of the exhumation rate in the Cordillera Blanca during the Quaternary (~0.2 km/Ma at 6 Ma to ~1 km/Ma at 2 Ma). The higher predicted exhumation rate correlates with area of higher relief (northern and central parts of the Cordillera Blanca). This suggests that valley carving and glaciations controlled the late stage of the Cordillera Blanca exhumation (2–0 Ma). Only the combined crustal-scale normal fault presence and recent high exhumation rates permitted to exhume the younger rocks emplaced deeper close to the CBNF. We show that the main phase of uplift and exhumation occurred several million years after the cessation of the magmatic activity in the Cordillera Blanca. Therefore, we propose that the magmatism does not represent a major contribution to the crustal thickening. One we would expect an uplift and exhumation phase to be recorded during the magmatic arc emplacement, which is not the case. Finally, our data suggest that the Miocene magmatic arc does not directly contribute to major crustal thickening nor to regional surface uplift and exhumation in northern

Peru. Late increase in exhumation rates in the Cordillera Blanca is the result of climate change, with the initiation of extensive glaciation during the Pleistocene, leading to rapid valley incision, uplift and increase of exhumation rates.

Recent tectonic and geomorphology contributions to the understanding of orogen-scale processes demonstrate the coupling of deformation and erosion in mountain ranges building [e.g., *Horton*, 1999; *Montgomery et al*., 2001; *Whipple and Meade*, 2004]. Even if displacements on crustal-scale normal faults have been considerably larger, in the Himalayas, for example [e.g., *Pêcher*, 1991; *Brunel et al*., 1994; *Searle et al*., 2006; *Kali et al*., 2010; *Thiede et al*., 2013], there is no evidence of large-scale extension in the central Andes except in the Cordillera Blanca region [e.g., *Dalmayrac and Molnar*, 1981; *Bonnot*, 1984; *McNulty and Farber*, 2002], which also includes the highest Peruvian peaks. The Cordillera Blanca batholith emplacement depth indicates a displacement of ~11 km on the CBNF for the last 5 Ma. The presence of the batholith localized the deformation and focused the $>$ 5000 m relief building. Moreover, consecutive glacial erosion of the Miocene magmatic arc contributes to its recent exhumation and also accelerated the relief building.

Acknowledgments
All amphibole thermobarometry data plotted in the figures can be founded in the supporting information; geochronological and thermochronological data can be obtained from the cited references. This work was supported by a grant from LabEx OSUG@2020 (Observatoire des Sciences de l'Univers de Grenoble, Investissements d'Avenir, ANR10 LABX56) and SMINGUE. We thank Valérie Magnin for her help during microprobe measurements. We thank the SERNAMP for allowing sampling in the Cordillera Blanca. We acknowledge the two anonymous reviewers for their constructive reviews that helped a lot to improve the manuscript.

References

Atherton, M. P., and L. M. Sanderson (1987), The Cordillera Blanca batholith: A study of granite intrusion and the relation of crustal thickening to peraluminosity, *Geol. Rundsch.*, *76*(1), 213–232.

Barnes, J. B., and J. D. Pelletier (2006), Latitudinal variation of denudation in the evolution of the Bolivian Andes, *Am. J. Sci.*, *306*, 1–31.

Beckinsale, R. D., A. W. Sanchez-Fernandez, M. Brook, E. J. Cobbing, W. P. Taylor, and N. B. Moore (1985), Rb-Sr whole rock isochron and K-Ar determination for the Coastal Batholith of Peru, in *Magmatism at a Plate Edge: The Peruvian Andes*, edited by W. S. Pitcher et al., pp. 177–202, Blackie Halstead press, Glasgow.

Boekhout, F., R. Spikings, T. Sempere, M. Chiaradia, A. Ulianov, and U. Schaltegger (2012), Mesozoic arc magmatism along the southern Peruvian margin during Gondwana breakup and dispersal, *Lithos*, *146–147*(C), 48–64, doi:10.1016/j.lithos.2012.04.015.

Bonnot, D. (1984), Néotectonique et tectonique active de la Cordillère Blanche et du Callejón de Huaylas (Andes nord-péruviennes), Unpublished PhD thesis, Université de Paris-Sud, Centre d'Orsay, France.

Bonnot, D., M. Sébrier, and J. Mercier (1988), Évolution géodynamique plio-quaternaire du bassin intra-cordillérain du Callejón de Huaylas et de la Cordillère Blanche, Pérou, *Geodynamique*, *3*(1–2), 57–83.

Braun, J., D. Zwartz, and J. H. Tomkin (1999), A new surface-processes model combining glacial and fluvial erosion, *Ann. Glaciol.*, *28*(1), 282–290.

Brenna, M., R. Price, S. J. Cronin, I. E. M. Smith, Y. K. Sohn, G. B. Kim, and R. Maas (2014), Final magma storage depth modulation of explosivity and trachyte-phonolite genesis at an intraplate volcano: A case study from Ulleung Island, South Korea, *J. Petrol.*, *55*(4), 709–747, doi:10.1093/petrology/egu004.

Brunel, M., N. Arnaud, P. Tapponnier, Y. Pan, and Y. Wang (1994), Kongur Shan normal fault: Type example of mountain building assisted by extension (Karakoram fault, eastern Pamir), *Geology*, *22*(8), 707–710.

Buck, W. R. (1988), Flexural rotation of normal faults, *Tectonics*, *7*(5), 959–973, doi:10.1029/TC007i005p00959.

Campani, M., F. Herman, and N. Mancktelow (2010), Two- and three-dimensional thermal modeling of a low-angle detachment: Exhumation history of the Simplon Fault Zone, central Alps, *J. Geophys. Res.*, *115*, B10420, doi:10.1029/2009JB007036.

Champagnac, J. D., P. Molnar, R. S. Anderson, C. Sue, and B. Delacou (2007), Quaternary erosion-induced isostatic rebound in the western Alps, *Geology*, *35*(3), 195–198, doi:10.1130/G23053A.1.

Clapperton, C. M. (1983), The glaciation of the Andes, *Quat. Sci. Rev.*, *2*, 83–155.

Cobbing, J., W. Pitcher, J. Baldock, W. Taylor, W. McCourt, and N. J. Snelling (1981), Estudio geológico de la Cordillera Occidental del norte del Perú, *Inst. Geol. Minero y Metall. Ser. D. Estud. Espec.*, *10*(D), 1–252.

Coldwell, B., J. Clemens, and N. Petford (2011), Deep crustal melting in the Peruvian Andes: Felsic magma generation during delamination and uplift, *Lithos*, *125*(1–2), 272–286, doi:10.1016/j.lithos.2011.02.011.

Costa, F., S. Andreastuti, C. B. de Maisonneuve, and J. S. Pallister (2013), Petrological insights into the storage conditions, and magmatic processes that yielded the centennial 2010 Merapi explosive eruption, *J. Volcanol. Geotherm. Res.*, *261*(C), 209–235, doi:10.1016/j.jvolgeores.2012.12.025.

Dalmayrac, B., and P. Molnar (1981), Parallel thrust and normal faulting in Peru and constraints on the state of stress, *Earth Planet. Sci. Lett.*, *55*, 473–481.

De Angelis, S. H., J. Larsen, and M. Coombs (2013), Pre-eruptive magmatic conditions at Augustine Volcano, Alaska, 2006: Evidence from Amphibole Geochemistry and Textures, *J. Petrol.*, *54*(9), 1939–1961, doi:10.1093/petrology/egt037.

Deverchère, J., C. Dorbath, and L. Dorbath (1989), Extension related to a high topography: Results from a microearthquake survey in the Andes of Peru and tectonic implications, *Geophys. J. Int.*, *98*(2), 281–292.

Egeler, C. G., and T. De Booy (1956), *Geology and Petrology of Part of the Southern Cordillera Blanca, Peru*, *Koninklijk Nederlands Geologisch Mijnbouwkundig Genootschap*, vol. 1–1, Mouton.

Erdmann, S., C. Martel, M. Pichavant, and A. Kushnir (2014), Amphibole as an archivist of magmatic crystallization conditions: Problems, potential, and implications for inferring magma storage prior to the paroxysmal 2010 eruption of Mount Merapi, Indonesia, *Contrib. Mineral Petrol.*, doi:10.1007/s00410-014-1016-4.

Farber, D. L., G. S. Hancock, R. C. Finkel, and D. T. Rodbell (2005), The age and extent of tropical alpine glaciation in the Cordillera Blanca, Peru, *J. Quat. Sci.*, *20*(7–8), 759–776, doi:10.1002/jqs.994.

Farrar, E., and D. C. Noble (1976), Timing of late Tertiary deformation in the Andes of Peru, *Geol. Soc. Am. Bull.*, *87*(9), 1247–1250.

Fox, M., F. Herman, S. D. Willett, and D. A. May (2014), A linear inversion method to infer exhumation rates in space and time from thermochronometric data, *Earth Surf. Dyn.*, *2*(1), 47–65, doi:10.5194/esurf-2-47-2014.

Garzione, C. N., P. Molnar, J. C. Libarkin, and B. J. MacFadden (2006), Rapid late Miocene rise of the Bolivian Altiplano: Evidence for removal of mantle lithosphere, *Earth Planet. Sci. Lett.*, *241*(3–4), 543–556, doi:10.1016/j.epsl.2005.11.026.

Gephart, J. W. (1994), Topography and subduction geometry in the central Andes: Clues to the mechanics of a noncollisional orogen, *J. Geophys. Res.*, *99*(B6), 12,279–12,288, doi:10.1029/94JB00129.

Giletti, B. J., and H. W. Day (1968), Potassium–Argon ages of igneous intrusive rocks in Peru, *Nature*, *220*(5167), 570–572, doi:10.1038/220570a0.
Giovanni, M. K. (2007), Tectonic and thermal evolution of the Cordillera Blanca detachment system, Peruvian Andes: Implication for normal faulting in a contractionnal orogen, *Unpublished* PhD thesis, University of California, Los Angeles, USA.
Giovanni, M. K., B. K. Horton, C. N. Garzione, B. McNulty, and M. Grove (2010), Extensional basin evolution in the Cordillera Blanca, Peru: Stratigraphic and isotopic records of detachment faulting and orogenic collapse in the Andean hinterland, *Tectonics*, *29*, TC6007, doi:10.1029/2010TC002666.
Herman, F., and M. T. Brandon (2015), Mid-latitude glacial erosion hotspot related to equatorial shifts in southern westerlies, *Geology*, *1–4*, doi:10.1130/G37008.1.
Herman, F., D. Seward, P. G. Valla, A. Carter, and B. Kohn (2013), Worldwide acceleration of mountain erosion under a cooling climate, *Nature*, doi:10.1038/nature12877.
Hodson, K. R. (2012), Morphology, exhumation, and Holocene erosion rates from a tropical glaciated mountain range: The Cordillera Blanca, Peru, Department of Earth & Planetary Sciences, *Unpublished M. S. thesis,* McGill University, Montreal, Canada.
Hoorn, C., et al. (2010), Amazonia through time: Andean uplift, climate change, landscape evolution, and biodiversity, *Science*, *330*(6006), 927–931, doi:10.1126/science.1194585.
Horton, B. K. (1999), Erosional control on the geometry and kinematics of thrust belt development in the central Andes, *Tectonics*, *18*(6), 1292–1304, doi:10.1029/1999TC900051.
Husson, L., and T. Sempéré (2003), Thickening the Altiplano crust by gravity-driven crustal channel flow, *Geophys. Res. Lett.*, *30*(5), 1243, doi:10.1029/2002GL016877.
INGEMMET (El Instituto Geológico Minero y Metalúrgico) (1999), Mapa geológico del Perú: Peru Instituto Geológico, Minero y Metalúrgico, Sector Energía y Minas, 1:1,000,000.
Isacks, B. L. (1988), Uplift of the central Andean plateau and bending of the Bolivian orocline, *J. Geophys. Res.*, *93*(B4), 3211–3231, doi:10.1029/JB093iB04p03211.
James, D. E. (1971), Plate tectonic model for the evolution of the central Andes, *Geol. Soc. Am. Bull.*, *82*, 3325–3346.
James, D. E., and I. S. Sacks (1999), Cenozoic formation of the central Andes: A geophysical perspective, in *Geology and Ore Deposits of the Central Andes*, vol. 7, edited by B. J. Skinner, Society of Economic Geologists.
James, D. E., and J. A. Snoke (1994), Structure and tectonics in the region of flat subduction beneath central Peru: Crust and uppermost mantle, *J. Geophys. Res.*, *99*(B4), 6899–6912, doi:10.1029/93JB03112.
Jordan, T. E., B. L. Isacks, R. W. Allmendinger, J. A. Brewer, V. A. Ramos, and C. J. Ando (1983), Andean tectonics related to geometry of subducted Nazca plate, *Geol. Study Am. Bull.*, *94*, 341–361.
Kali, E., P. H. Leloup, N. Arnaud, G. Mahéo, D. Liu, E. Boutonnet, J. Van Der Woerd, X. Liu, J. Liu-Zeng, and H. Li (2010), Exhumation history of the deepest central Himalayan rocks, Ama Drime range: Key pressure-temperature-deformation-time constraints on orogenic models, *Tectonics*, *29*, TC2014, doi:10.1029/2009TC002551.
Kiss, B., S. Harangi, T. Ntaflos, P. R. D. Mason, and E. Pál-Molnár (2014), Amphibole perspective to unravel pre-eruptive processes and conditions in volcanic plumbing systems beneath intermediate arc volcanoes: A case study from Ciomadul volcano (SE Carpathians), *Contrib. Mineral. Petrol.*, *167*(3), 1–27, doi:10.1007/s00410-014-0986-6.
Kley, J., and C. R. Monaldi (1998), Tectonic shortening and crustal thickness in the central Andes: How good is the correlation?, *Geology*, *26*(8), 723–726.
Kley, J., C. R. Monaldi, and J. A. Salfity (1999), Along-strike segmentation of the Andean foreland: Causes and consequences, *Tectonophysics*, *301*(1), 75–94.
Kono, M., Y. Fukao, and A. Yamamoto (1989), Mountain building in the central Andes, *J. Geophys. Res.*, *94*(B4), 3891–3905, doi:10.1029/JB094iB04p03891.
Kusznir, N. J., G. Marsden, and S. S. Egan (1991), A flexural cantilever simple-shear/pure-shear model of continental extension, in *The Geometry of Normal Faults*, edited by A. M. Roberts et al., *Geol. Soc., London, Spec. Publ.*, *56*, 41–60.
Lamb, S., and L. Hoke (1997), Origin of the high plateau in the central Andes, Bolivia, South America, *Tectonics*, *16*(4), 623–649, doi:10.1029/97TC00495.
Lamb, S., and P. Davis (2003), Cenozoic climate change as a possible cause for the rise of the Andes, *Nature*, *425*(6960), 792–797.
Leake, B. E., et al. (1997), Nomenclature of the amphiboles: Report of the subcommittee on amphiboles of the International Mineralogical Association, Commission on New Minerals and Mineral Names, *Am. Mineral.*, *82*, 1019–1037.
Leuthold, J., O. Müntener, L. P. Baumgartner, B. Putlitz, M. Ovtcharova, and U. Schaltegger (2012), Time resolved construction of a bimodal laccolith (Torres del Paine, Patagonia), *Earth Planet. Sci. Lett.*, *325–326*(C), 85–92, doi:10.1016/j.epsl.2012.01.032.
Leuthold, J., O. Muntener, L. P. Baumgartner, and B. Putlitz (2014), Petrological constraints on the recycling of mafic crystal mushes and intrusion of braided sills in the Torres del Paine Mafic Complex (Patagonia), *J. Petrol.*, *55*(5), 917–949, doi:10.1093/petrology/egu011.
Mamani, M., G. Wörner, and T. Sempéré (2010), Geochemical variations in igneous rocks of the Central Andean orocline (13°S to 18°S): Tracing crustal thickening and magma generation through time and space, *Geol. Soc. Am. Bull.*, *122*(1–2), 162–182, doi:10.1130/B26538.1.
Margirier, A., X. Robert, L. Audin, C. Gautheron, M. Bernet, S. Hall, and T. Simon-Labric (2015), Slab flattening, magmatism and surface uplift in the Cordillera Occidental (northern Peru), *Geology*, *43*(11), 1031–1034, doi:10.1130/G37061.1.
Masek, J. G., B. L. Isacks, and T. L. Gubbels (1994), Erosion and tectonics at the margins of continental plateaus, *J. Geophys. Res.*, *99*(B7), 13,941–13,956, doi:10.1029/94JB00461.
McNulty, B. A., and D. L. Farber (2002), Active detachment faulting above the Peruvian flat slab, *Geology*, *30*(6), 567–570.
McNulty, B. A., D. L. Farber, G. S. Wallace, R. Lopez, and O. Palacios (1998), Role of plate kinematics and plate-slip-vector partitioning in continental magmatic arcs: Evidence from the Cordillera Blanca, Peru, *Geology*, *26*(9), 827–830.
McQuarrie, N. (2002), The kinematic history of the central Andean fold-thrust belt, Bolivia: Implications for building a high plateau, *Geol. Soc. Am. Bull.*, *114*(8), 950–963.
Michalak, M. J., S. R. Hall, D. L. Farber, L. Audin, and J. K. Hourigan (2016), (U-Th)/He thermochronology records late Miocene accelerated cooling in the north-central Peruvian Andes, *Lithosphere*, *8*(2), 103–115.
Montario, M. J. (2001), Exhumation of the Cordillera Blanca, Northern Peru, based on apatite fission track analysis, Departement of Geology, Unpublished thesis, Union College, Schenectady, New York, USA.
Montario, M. J. (2006), Thermochronological evidence for Neogene incision of the Rio Pativilca Canyon, northern Peru, Department of Geology, Unpublished M.S. thesis, Univ. at Albany, State Univ. of New York, USA.
Montgomery, D. R. (2002), Valley formation by fluvial and glacial erosion, *Geology*, *30*(11), 1047–1050.
Montgomery, D. R., G. Balco, and S. D. Willett (2001), Climate, tectonics, and the morphology of the Andes, *Geology*, *29*(7), 579–582.

Mukasa, S. B. (1984), Comparative Pb isotope systematics and zircon U-Pb geochronology for the Coastal, San Nicolás and Cordillera Blanca Batholiths, Peru, *Unpublished PhD thesis*, Univ. of California, Santa Barbara, USA.
Mukasa, S. B., and G. R. Tilton (1984), Lead isotope systematics in batholithic rocks of the western and coastal cordilleras, Peru, in *Andean Magmatism*, pp. 180–189, Birkhäuser, Boston.
Pêcher, A. (1991), The contact between the Higher Himalaya Crystallines and the Tibetan Sedimentary Series: Miocene large-scale dextral shearing, *Tectonics*, *10*(3), 587–598, doi:10.1029/90TC02655.
Pérez-Gussinyé, M., C. J. Swain, J. F. Kirby, and A. R. Lowry (2009), Spatial variations of the effective elastic thickness, Te, using multitaper spectral estimation and wavelet methods: Examples from synthetic data and application to South America, *Geochem. Geophys. Geosyst.*, *10*, Q04005, doi:10.1029/2008GC002229.
Petford, N., and M. Atherton (1996), Na-rich partial melts from newly underplated basaltic crust: The Cordillera Blanca Batholith, Peru, *J. Petrol.*, *37*(6), 1491–1521.
Petford, N., and M. P. Atherton (1992), Granitoid emplacement and deformation along a major crustal lineament: The Cordillera Blanca, Peru, *Tectonophysics*, *205*(1), 171–185.
Pope, D. C., and S. D. Willett (1998), Thermal-mechanical model for crustal thickening in the central Andes driven by ablative subduction, *Geology*, *26*(6), 511, doi:10.1130/0091-7613(1998)026<0511:TMMFCT>2.3.CO;2.
Putirka, K. (2014), Amphibole-liquid equilibria: Barometers and thermometers for volcanic systems, 2014 GSA Annual Meeting in Vancouver.
Ridolfi, F., and A. Renzulli (2012), Calcic amphiboles in calc-alkaline and alkaline magmas: Thermobarometric and chemometric empirical equations valid up to 1,130°C and 2.2 GPa, *Contrib. Mineral. Petrol.*, *163*(5), 877–895, doi:10.1007/s00410-011-0704-6.
Ridolfi, F., A. Renzulli, and M. Puerini (2010), Stability and chemical equilibrium of amphibole in calc-alkaline magmas: An overview, new thermobarometric formulations and application to subduction-related volcanoes, *Contrib. Mineral. Petrol.*, *160*(1), 45–66, doi:10.1007/s00410-009-0465-7.
Ridolfi, F., R. Braga, B. Cesare, A. Renzulli, D. Perugini, and S. Del Moro (2016), Unravelling the complex interaction between mantle and crustal magmas encoded in the lavas of San Vincenzo (Tuscany, Italy). Part I: Petrography and Thermobarometry, *Lithos*, *244*(C), 218–232, doi:10.1016/j.lithos.2015.09.029.
Rodbell, D. T. (1993), Subdivision of late Pleistocene moraines in the Cordillera Blanca, Peru, based on rock-weathering features, soils, and radiocarbon dates, *Quat. Res.*, *39*, 133–143.
Schildgen, T. F., K. V. Hodges, K. X. Whipple, P. W. Reiners, and M. S. Pringle (2007), Uplift of the western margin of the Andean plateau revealed from canyon incision history, southern Peru, *Geology*, *35*(6), 523, doi:10.1130/G23532A.1.
Schwartz, D. P. (1988), Paleoseismicity and neotectonics of the Cordillera Blanca fault zone, northern Peruvian Andes, *J. Geophys. Res.*, *93*(B5), 4712–4730, doi:10.1029/JB093iB05p04712.
Searle, M. P. (1999), Emplacement of Himalayan leucogranites by magma injection along giant sill complexes: Examples from the Cho Oyu, Gyachung Kang and Everest leucogranites (Nepal Himalaya), *J. Asian Earth Sci.*, *17*, 773–783.
Searle, M. P., R. D. Law, and M. J. Jessup (2006), Crustal structure, restoration and evolution of the Greater Himalaya in Nepal-South Tibet: Implications for channel flow and ductile extrusion of the middle crust, *Geol. Soc. Lond. Spec. Publ.*, *268*, 355–378.
Shane, P., and V. C. Smith (2013), Using amphibole crystals to reconstruct magma storage temperatures and pressures for the post-caldera collapse volcanism at Okataina volcano, *Lithos*, *156–159*(C), 159–170, doi:10.1016/j.lithos.2012.11.008.
Siame, L. L., M. Sébrier, O. Bellier, and D. Bourles (2006), Can cosmic ray exposure dating reveal the normal faulting activity of the Cordillera Blanca Fault, Peru?, *Rev. Asoc. Geol. Argent.*, *61*(4), 536–544.
Sisson, T. W., T. L. Grove, and D. S. Coleman (1996), Hornblende gabbro sill complex at Onion Valley, California, and a mixing origin for the Sierra Nevada batholith, *Contrib. Mineral. Petrol.*, *126*(1–2), 81–108, doi:10.1007/s004100050237.
Smith, J. A., R. C. Finkel, D. L. Farber, D. T. Rodbell, and G. O. Seltzer (2005), Moraine preservation and boulder erosion in the tropical Andes: Interpreting old surface exposure ages in glaciated valleys, *J. Quat. Sci.*, *20*(7–8), 735–758, doi:10.1002/jqs.981.
Stewart, J. W., J. F. Evernden, and N. J. Snelling (1974), Age determinations from Andean Peru: A reconnaissance survey, *Geol. Soc. Am. Bull.*, *85*(7), 1107–1116.
Thiede, R. C., E. R. Sobel, J. Chen, L. M. Schoenbohm, D. F. Stockli, M. Sudo, and M. R. Strecker (2013), Late Cenozoic extension and crustal doming in the India-Eurasia collision zone: New thermochronologic constraints from the NE Chinese Pamir, *Tectonics*, *32*, 763–779, doi:10.1002/tect.20050.
Turner, S. J., P. Izbekov, and C. Langmuir (2013), The magma plumbing system of Bezymianny Volcano: Insights from a 54 year time series of trace element whole-rock geochemistry and amphibole compositions, *J. Volcanol. Geotherm. Res.*, *263*, 108–121, doi:10.1016/j.jvolgeores.2012.12.014.
Valla, P. G., D. L. Shuster, and P. A. van der Beek (2011), Significant increase in relief of the European Alps during mid-Pleistocene glaciations, *Nat. Geosci.*, *4*(10), 688–692, doi:10.1038/ngeo1242.
Walker, B. A., E. W. Klemetti, A. L. Grunder, J. H. Dilles, F. J. Tepley, and D. Giles (2012), Crystal reaming during the assembly, maturation, and waning of an eleven-million-year crustal magma cycle: Thermobarometry of the Aucanquilcha Volcanic Cluster, *Contrib. Mineral. Petrol.*, *165*(4), 663–682, doi:10.1007/s00410-012-0829-2.
Whipple, K. X., and B. J. Meade (2004), Controls on the strength of coupling among climate, erosion, and deformation in two-sided, frictional orogenic wedges at steady state, *J. Geophys. Res.*, *109*, F01011, doi:10.1029/2003JF000019.
Wilson, P. A. (1975), K-Ar age studies in Peru with special reference to the emplacement of the Coastal Batholith, Unpublished PhD thesis, University of Liverpool, Liverpool, England.
Wipf, M. (2006), Evolution of the Western Cordillera and Coastal Margin of Peru: Evidence from low-temperature thermochronology and geomorphology, Unpublished PhD thesis, Swiss Federal Institute of Technology Zürich, Switzerland.
Wise, J. M., and D. C. Noble (2003), Geomorphic evolution of the Cordillera Blanca, Northern Peru, *Bol. Soc. Geol. Peru*, *96*, 1–21.
Zandt, G., A. A. Velasco, and S. L. Beck (1994), Composition and thickness of the southern Altiplano crust, Bolivia, *Geology*, *22*(11), 1003–1006.
Zhang, P., P. Molnar, and W. R. Downs (2001), Increased sedimentation rates and grain sizes 2–4 Myr ago due to the influence of climate change on erosion rates, *Nature*, *410*, 891–897.